Anisotropic magnetic properties and magnetic structure of YbPdSi

2016 J. Phys.: Condens. Matter 28 336002

(http://iopscience.iop.org/0953-8984/28/33/336002)

IOP Publishing Journal of Physics: Condensed Matter
J. Phys.: Condens. Matter **28** (2016) 336002 (11pp) doi:10.1088/0953-8984/28/33/336002

Anisotropic magnetic properties and magnetic structure of YbPdSi

Naohito Tsujii[1], Lukas Keller[2], Andreas Dönni[1] and Hideaki Kitazawa[1]

[1] National Institute for Materials Science, 1-2-1 Sengen, Tsukuba 305-0047, Japan
[2] Laboratory for Neutron Scattering and Imaging, Paul Scherrer Institut, CH-5232 Villigen, PSI, Switzerland

E-mail: tsujii.naohito@nims.go.jp

Received 29 March 2016, revised 29 May 2016
Accepted for publication 31 May 2016
Published 28 June 2016

Abstract

YbPdSi with orthorhombic crystal structure (space group *Pmmn*) exhibits a magnetic transition at $T_m = 8$ K, below which a ferromagnetic moment develops with an enhanced electronic specific-heat coefficient $\gamma \sim 200$ mJ K^{-2} mol^{-1}. We have investigated the magnetization, electrical resistivity, and specific heat of YbPdSi using single crystalline samples as functions of temperature and magnetic field. It has been found that the ferromagnetic moment points to the *c*-direction, although the magnetic moments have an Ising-like anisotropy along the *b*-direction above the magnetic-transition temperature. Field dependence of the magnetization and electrical resistivity shows a metamagnetic-like transition at $H_m = 0.3$ T when field is applied along the *b*-axis below $T = 3$ K, suggesting the existence of an antiferromagnetic component along this direction. The magnetic structure has been investigated by neutron diffraction using powder samples. The magnetic unit cell is identical to the crystal unit cell. The Rietveld fitting has revealed that Yb at the 2*a* and 2*b* positions exhibit a collinear ferromagnetic order along the *c*-axis, whereas Yb at the 4*e* position undergoes a non-collinear order, involving the ferromagnetic moment along the *c*-axis and an antiferromagnetic component along the *b*-axis. The ferromagnetic moments determined by the neutron diffraction are 0.26, 1.3, and 0.15 μ_B for Yb at the 4*e*, 2*b*, and 2*a* sites, respectively. The reduced moments for the 4*e* and the 2*a* sites suggest that the Kondo screening effect is important in YbPdSi.

Keywords: Kondo lattice compounds, ferromagnetic, metamagnetic, neutron diffraction, magnetic structure

S Online supplementary data available from stacks.iop.org/JPhysCM/28/336002/mmedia

(Some figures may appear in colour only in the online journal)

1. Introduction

A great deal of research has been devoted to understand the physics at the quantum critical point (QCP), where the magnetic ordered state vanishes because of the competition of the Kondo effect and the Rudermann–Kittel–Kasuya–Yosida interaction [1–4]. Novel phenomena such as unconventional superconductivity and non-Fermi liquid behavior have been found in the vicinity of QCP. For most of those phenomena, antiferromagnetic spin fluctuations appear to be responsible. Recently, however, it has been suggested that ferromagnetic correlation plays an important role in some compounds. For example, UGe_2 [5], URhGe [6, 7], and UCoGe [8] show coexistence of ferromagnetic ordering and superconductivity. Notably, this superconducting phase evolves inside the ferromagnetic ordered region. To shed light on the correlation between the ferromagnetic fluctuation and the superconducting state, it is important to investigate the electronic state of ferromagnetic Kondo-lattice compounds, especially those close to the ferromagnetic quantum critical point.

Recently, we reported magnetic properties of YbPdSi using polycrystalline samples. YbPdSi belongs to the large

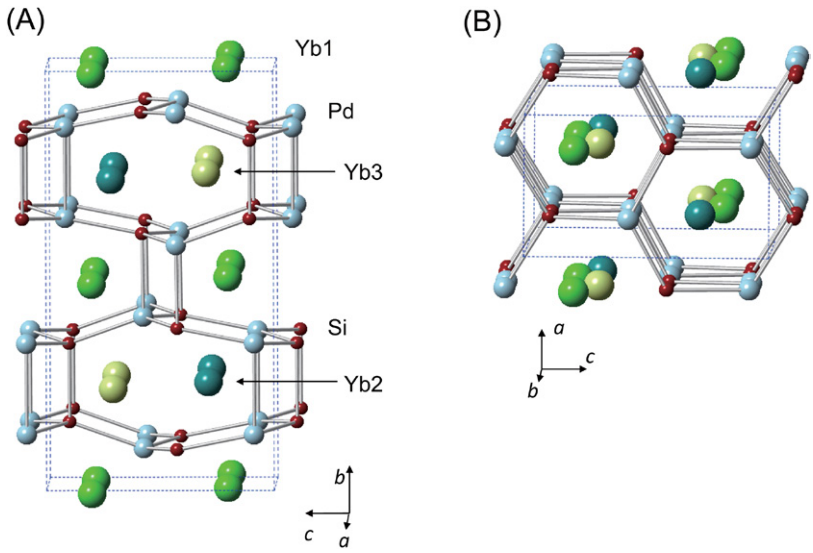

Figure 1. Crystal structure of YbPdSi.

RTX-family (R = rare earths, T = transition metal elements, and X = IIIA, IVA, VA elements), which displays quite a rich variety of magnetic properties [9]. We showed that YbPdSi can be an example of ferromagnetic heavy-fermion compounds [10]. YbPdSi crystallizes in the orthorhombic YPdSi-type structure, space group *Pmmn* [11]. The crystal structure is shown in figure 1. It is derived from the tetragonal $CeCu_2$-type (KHg_2-type) structure. Both of the $CeCu_2$-type and the YPdSi-type structures involve a puckered honeycomb layer within the *ac*-plane. While the $CeCu_2$-type structure has only one rare earth site, the YPdSi-type structure involves three rare earth sites because of three bondings of Pd–Si, Pd–Pd, and Si–Si along the *b*-axis. The magnetization measurements using polycrystalline samples revealed that ferromagnetic moments develop below $T = 8$ K [10]. The ordered state is accompanied by an enhanced electronic specific heat coefficient, suggesting a heavy fermion state. Indeed, the magnetic entropy of YbPdSi only reaches 2/3 of $R\ln 2$ at T_C. These facts indicate that YbPdSi can be a ferromagnetic Kondo-lattice system, where ferromagnetic ordered moments are suppressed by the Kondo effect.

Several Yb-based compounds with related crystal structures exhibit ferromagnetic behavior with an enhanced mass. For example, YbNiSn and YbPtGe crystallize in the TiNiSi-type structure. These have been known as classic examples of ferromagnetic Kondo lattices, with $T_C = 5.5$ K and 5.4 K and the electronic specific heat coefficient $\gamma = 300$ and 209 mJ K^{-2} mol^{-1}, respectively [12–14]. Another example is YbPdGe with the tetragonal YbAuSn-type structure [15], which undergoes a ferromagnetic transition at $T_C = 11.4$ K, below which a moderate heavy fermion state with $\gamma =$ 150 mJ K^{-2} mol^{-1} was observed [16]. Interestingly, magnetism of these compounds are not simple ferromagnetic. While YbPtGe exhibits ferromagnetic moments along the *c*-axis, antiferromagnetic-like behavior was observed for the other directions [14, 17]. Similar anisotropy was also observed for YbNiSn [12] and YbPdGe [16, 18]. Indeed, neutron powder diffraction experiments on YbPtGe and YbPdGe have demonstrated that the magnetic structures involve both of the ferromagnetic and weak antiferromagnetic components [18]. Therefore, it was suggested that the origin of the heavy fermion behavior can partly be due to the fluctuation of the antiferromagnetic components in these ferromagnetic Kondo-lattice compounds.

For the case of YbPdSi, the previous investigation was done using polycrystalline samples. Therefore, detailed magnetic studies are called for to shed light on the origin of the heavy mass in the ordered state of YbPdSi. In this paper, we investigate the anisotropy of the magnetization and the electrical resistivity of YbPdSi using single crystalline samples. We confirmed a magnetic transition takes place at $T_m = 8$ K, below which ferromagnetic moments along the *c*-direction develop. Moreover, we show that an antiferromagnetic component also exists along the *b*-direction, as observed by the existence of metamagnetic-like behavior and a cusp in the magnetoresistance for the magnetic field $H \| b$. We carried out neutron powder diffraction experiments on YbPdSi and indeed clarified the existence of the antiferromagnetic component. Therefore, YbPdSi undergoes a non-collinear magnetic order, which seems to be a common feature in the Yb*TX* compounds with the $CeCu_2$-related crystal structures. In addition, reduced ordered moments were observed by the neutron diffraction, which implies the Kondo screening effect plays a dominant role.

2. Experimental method

Samples of YbPdSi were synthesized by melting PdSi and Yb in sealed tantalum tubes. First, Pd (99.95%) and Si (99.9999%) were arc-melted to make PdSi in an argon atmosphere. Then PdSi and Yb ingots (99.9%) were sealed in a tantalum tube using the arc furnace under argon. The tantalum tube was heated up to 1773 K using an induction furnace under vacuum, held at this temperature for 30 min, and cooled to 1073 K in 6 h. Single crystalline samples of YbPdSi were isolated from the melted ingot.

Magnetization was measured with a superconducting quantum interference device magnetometer (MPMS-5S, Quantum Design). Electrical resistivity and specific heat

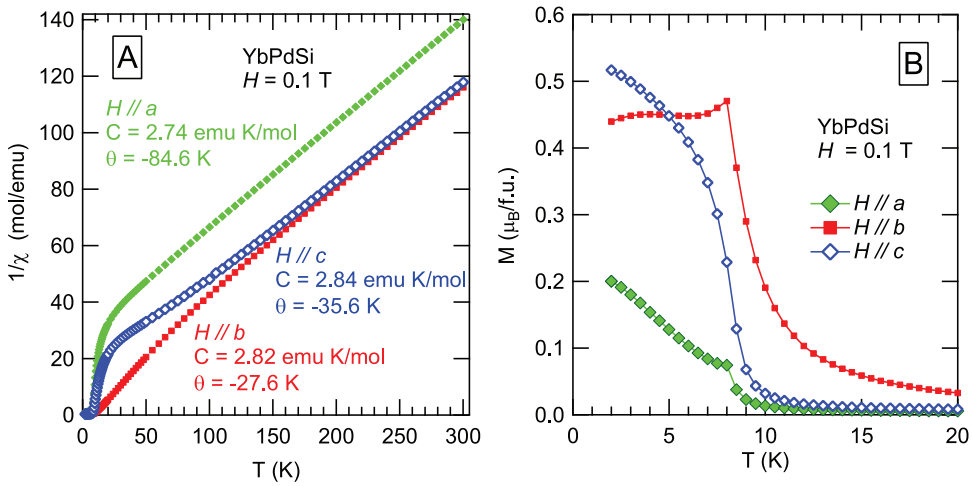

Figure 2. (A) Inverse of the magnetic susceptibility of YbPdSi, H/M, as a function of temperature T measured under the magnetic field of $H = 0.1$ T. Data along the a-, b-, and c-directions are plotted with filled diamonds, filled squares, and open diamonds, respectively. (B) Low temperature part of the magnetic susceptibility M/H of YbPdSi as a function of T.

under magnetic fields were measured with a physical property measurement system (PPMS, Quantum Design).

Neutron powder diffraction of YbPdSi was investigated to determine the magnetic structure. Neutron diffraction patterns were collected at the cold neutron powder diffractometer (DMC) of the Paul Scherrer Institute (PSI). Powder samples of 8 g were prepared by melting PdSi and Yb in tantalum tubes sealed under argon. The powder specimen was loaded in a vanadium sample holder and sealed under a helium atmosphere. The sample was cooled down to 1.5 K using a helium cryostat. The neutron diffraction measurements were carried out from 1.5 K up to 15 K with the neutron wavelength of $\lambda = 2.4565(2)$ Å The diffraction patterns were analyzed by the Rietveld method using the FullProf Suite software [19]. Possible models for the magnetic structure were deduced based on a group theory analysis using the SARAh software [20].

3. Results and discussion

3.1. Magnetic properties

In figure 2(A), temperature dependence of the reciprocal magnetic susceptibility H/M of YbPdSi is shown. For all the crystallographic directions, H/M show linear temperature dependence above 200 K, indicating the Curie–Weiss relation. The Curie constants C and the Weiss temperatures θ were obtained by fitting the data above 200 K, and the values are $C = 2.74$, 2.82, and 2.84 emu K mol^{-1}, and $\theta = -84.6$, -27.6, and -35.6 K for H parallel to the a-, b-, and c-directions, respectively. These values of the Curie constant correspond to the effective magnetic moments of $\mu_{\rm eff} = 4.7$ to 4.8 $\mu_{\rm B}$, which are close to the theoretical value $\mu_{\rm eff} = 4.54\,\mu_{\rm B}$ for a free Yb^{3+} ion. Magnetic susceptibility above 200 K along the c- and the b-axes are slightly larger than that along the a-axis, suggesting an XY-type anisotropy in the bc-plane. Below about 100 K, the magnetic susceptibility along the b-axis develops with the decrease of temperature, suggesting an Ising-like anisotropy along the b-axis. This change of the magnetic anisotropy suggests the crystalline electric field splittings of the Yb^{3+} state at around 100 K. This is consistent with the previous specific heat data of YbPdSi, which suggested that the $J = 7/2$ state of the Yb^{3+} ion splits into four doublets, and the energy separation between the ground and the first excited states is about 95 K [10].

The b-direction is perpendicular to the honeycomb layer formed by Pd and Si. It is notable that related compounds YbNiSn, YbPdGe, and YbPdGe in the paramagnetic region also show Ising-like anisotropies perpendicular to the $T - X$ honeycomb layer (T is transition metals, and X = Ge or Sn) [12, 14, 16].

Figure 2(B) shows the magnetic susceptibility M/H of YbPdSi below 20 K measured at $H = 0.1$ T as a function of T. For $H\|c$, M/H steeply increases below $T_{\rm m} = 8$ K, corresponding to the magnetic ordering. On the other hand, M/H for $H\|b$ exhibits a cusp at $T_{\rm m}$, and gradually decreases below this temperature. For the case of $H\|a$, M/H increases linearly with a very small anomaly at 8 K. These results suggest that the ferromagnetic moment points to the c-direction, and an antiferromagnetic component can also exist along the b-direction or in the ab-plane.

In figure 3, field dependence of the magnetization M of YbPdSi is displayed. M along the c-direction in figure 3(C) shows the evolution of ferromagnetic moments below 8 K. The spontaneous magnetization at 2 K is 0.5 $\mu_{\rm B}$ per Yb ion. For $H\|a$ (shown in figure 3(A)), M increases with a convex curve against H, indicating the absence of ferromagnetic component along the a-axis. For $H\|b$ shown in figure 3(B), M shows a linear increase at low fields, and saturates above 0.5 T with the magnetic moment of $M = 1.7$ $\mu_{\rm B}$. This value is much larger than the spontaneous moment along the c-direction, $M = 0.5$ $\mu_{\rm B}$. This reflects the Ising-like anisotropy of the magnetic moment along the b-direction.

In order to investigate the origin of the antiferromagnetic-like anomaly in YbPdSi along the b-direction, magnetic susceptibility and the field dependent magnetization were measured in more detail. Figure 4 shows the magnetic susceptibility M/H of YbPdSi along the b-direction measured under several

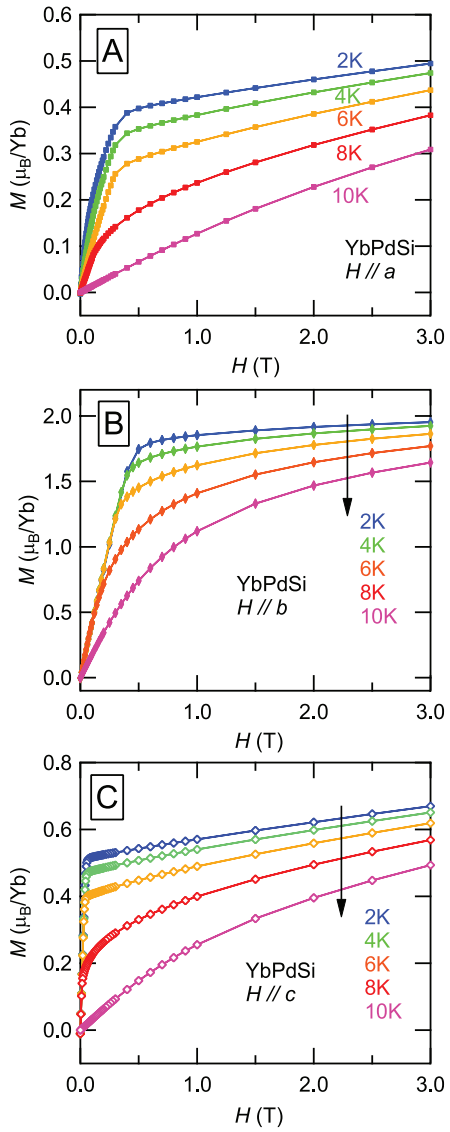

Figure 3. Field dependence of the magnetization M of YbPdSi measured with magnetic fields parallel to the a-, b-, and c-directions at various temperatures.

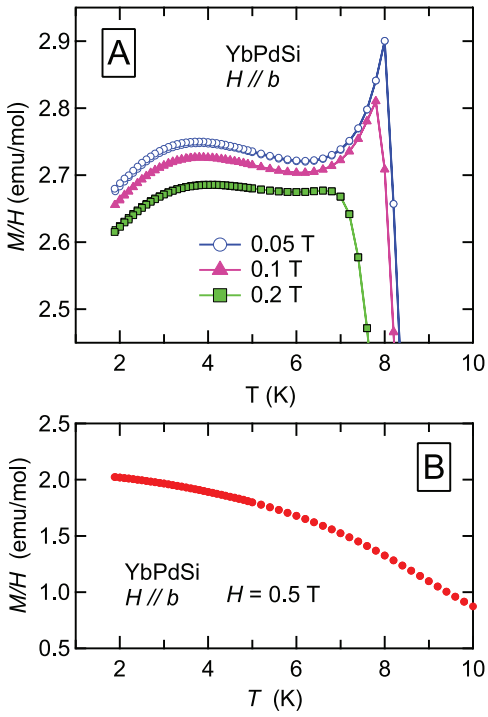

Figure 4. Magnetic susceptibility M/H of YbPdSi for fields $H\|b$ at low temperature measured under $H \leqslant 0.2$ T (A), and under $H = 0.5$ T (B).

magnetic fields. At $H = 0.05$ T, M/H shows a sharp cusp at $T_m = 8$ K, pointing to the magnetic transition with possible antiferromagnetic component along the b-direction. Below 8 K, M/H decreases and shows a broad maximum at 3 K. The origin of this anomaly is not clear, but possibly related to the development of the antiferromagnetic correlation. When the external field is increased, the cusp at T_m and the maximum at 3 K become vague. As displayed in figure 4(B), M/H at $H = 0.5$ T shows a monotonic increase with the decrease of T.

Figure 5 shows the field dependent magnetization M of YbPdSi and its derivative by field, dM/dH, along the b-direction. M at 2 K shows a very weak metamagnetic anomaly at 0.28 T, as indicated by the maximum in the dM/dH curve at 2 K. This anomaly vanishes above 3 K, and M increases linearly up to 0.3 T, above which M shows a saturation behavior. The weak metamagnetic behavior is indicative of a spin-flop transition: at low fields ($H \leqslant 0.28$ T), the ferromagnetic moment points to the c-direction with an antiferromagnetic component possibly lying along the b-direction, while at higher fields ($H \geqslant 0.28$ T), the magnetic moments are aligned toward the b-direction, and tend to be saturated with the increase of fields. It is notable that the maximum in dM/dH is only seen below 3 K, and the magnetic susceptibility at low fields show a broad maximum at 3.5 K as shown in figure 4(A). These results suggest that the broad maximum in M/H at $T = 3.5$ K for $H\|b$ can be related to the development of antiferromagnetic correlations along the b-direction.

3.2. Electrical resistivity

In figure 6, temperature dependence of the electrical resistivity ρ of YbPdSi is presented. An electrical current was applied along the a-direction. ρ shows a gradual decrease from room temperature and exhibits a broad minimum at 250 K, indicating the effect of Kondo interaction. Then ρ occurs a maximum at 80 K, suggesting the presence of crystal-field splitting of the $4f$ level, below which ρ decreases with a convex temperature dependence. A shoulder in ρ at $T_m = 8$ K corresponds to the magnetic transition. Below T_m, ρ decreases with a concave curvature against T. The lowest regions were well fit with a T^2 dependence, as will be shown later.

$\rho - T$ at low temperature under magnetic fields are plotted in figure 7. The shoulder at $T_m = 8$ K becomes vague under magnetic fields. The resistivity ρ at T_m decreases rapidly with increasing fields. Plotted in the inset of figure 7 is the magnetoresistance(MR) ratio, $\rho(H)/\rho(H = 0)$, at $T = 1.85$, 8 and 10 K. The MR ratio is largest for $T = 8$ K, since the

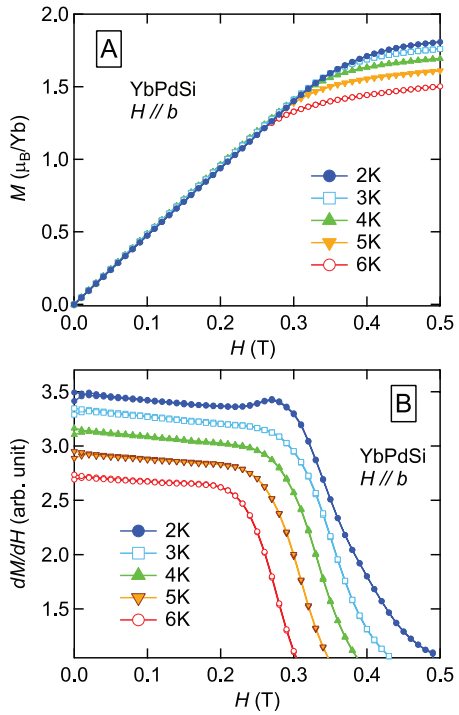

Figure 5. Magnetization M of YbPdSi under fields H parallel to the b direction (A), and its field derivative dM/dH measured at various temperatures (B).

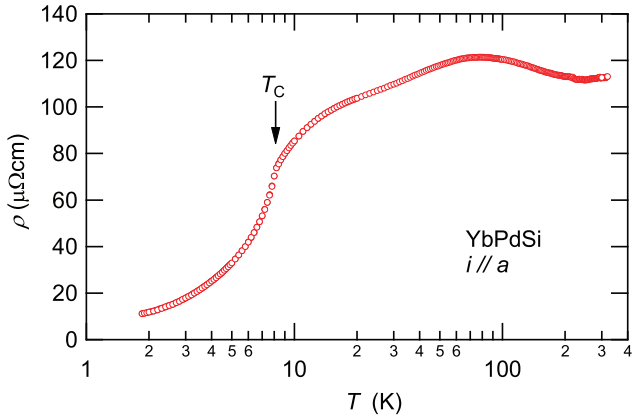

Figure 6. Electrical resistivity of YbPdSi as a function of temperature measured with a current along the a-direction.

magnetic fluctuation is most significantly suppressed by external fields at the ordering temperature.

In figure 8, electrical resistivity of YbPdSi measured with a current $i\|a$ under magnetic fields $H\|c$ is plotted as functions of T^2. Resistivity was fit with the function $\rho = \rho_0 + AT^2$, where ρ_0 is the residual resistivity and A is a coefficient. The results of the fitting are plotted in figure 8 with solid lines. It is clear that ρ are well described by a T^2 law, which is a characteristic behavior of Fermi-liquid systems. Inset of figure 8 shows the field variation of the T^2-coefficient A. The value of A shows a gradual decrease with the increase of H. In the Fermi-liquid theory, the parameter A is proportional to m^{*2}, where m^* is the effective mass of electrons [21]. Thus, the gradual decrease of A with H indicates that the electron-electron correlation in YbPdSi becomes weakened under magnetic fields.

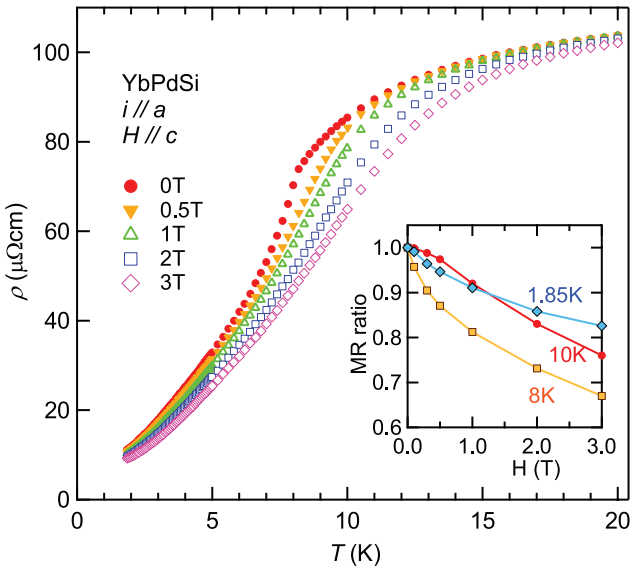

Figure 7. Electrical resistivity ρ of YbPdSi below 20 K measured under magnetic fields applied parallel to the c-direction with a current along the a direction. Inset shows the magnetoresistance ratio $\rho(H)/\rho(H=0)$ as a function of magnetic field.

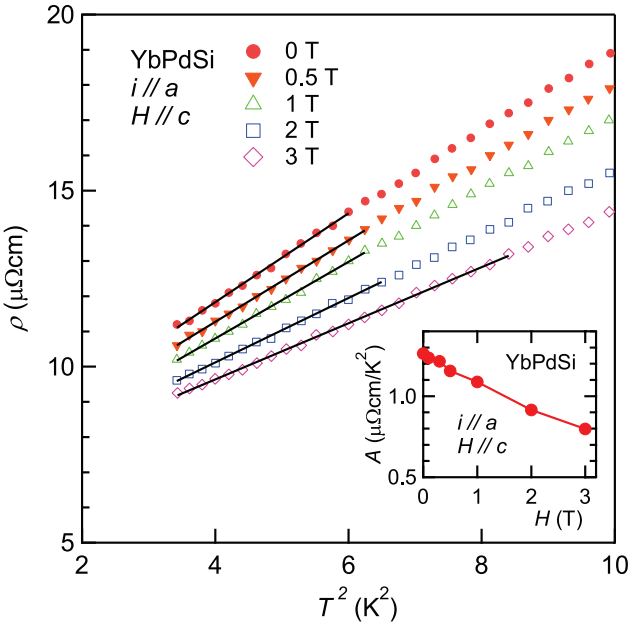

Figure 8. Electrical resistivity of YbPdSi measured with a current $i\|a$ under magnetic fields $H\|c$ as a function of the square of temperature T^2. Solid lines are the results of fitting with the function $\rho = \rho_0 + AT^2$, where ρ_0 is the residual resistivity and A is a parameter. Inset shows the magnetic field dependence of the parameter A obtained by the fitting.

Plotted in figure 9 is the $\rho - T$ curve of YbPdSi measured with a current $i\|a$ under magnetic fields $H\|b$. The kink at $T_m = 8$ K is rapidly suppressed by fields, similarly to the case of $H\|c$. The resistivity decreases by the application of magnetic fields, more significantly than the case of $H\|c$, shown in figure 7. This tendency is more evident in the MR ratio, which is presented in the inset of figure 9. The MR ratio for $H\|b$ decreases 40–60% at $H = 3$ T, much larger than the decrease for $H\|c$, 20–30% at the same field. This large MR is attributed

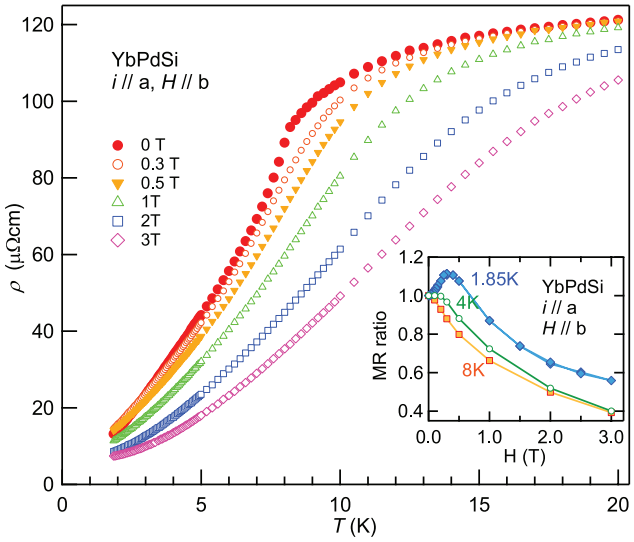

Figure 9. Electrical resistivity ρ of YbPdSi measured with a current $i \| a$ under magnetic fields parallel to the b-direction as a function of temperature. Inset shows the field dependence of the magnetoresistance ratio, $\rho(H)/\rho(H=0)$ at different temperatures.

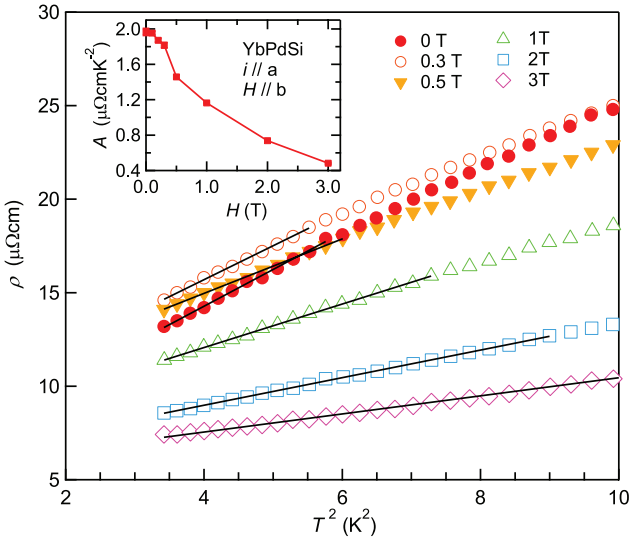

Figure 10. Electrical resistivity ρ as a function of the square of temperature T^2 measured with a current parallel to the a-direction under magnetic fields parallel to the b-direction. Solid lines represent the fit with a function $\rho = \rho_0 + AT^2$, where ρ_0 is the residual resistivity and A is a constant. Inset shows the field dependence of the value A obtained by the fitting.

to the larger saturated magnetization for $H\|b$ than for $H\|c$ as shown in figure 3, since the larger magnetization has the smaller magnetic scattering in the electrical conductivity. The field dependence of the MR for $H\|b$ exhibits a maximum at $H = 0.3$ T for $T = 1.85$ K. This is in contrast to the monotonic decrease of the MR for $H\|c$ (figure 7, inset). This behavior is consistent with the metamagnetic behavior only observed for $H\|b$ as shown in figure 5(B).

Figure 10 shows the resistivity ρ at low temperature under magnetic fields $H\|b$ plotted as functions of T^2. Solid lines in the figure represent the results of the fit with $\rho = \rho_0 + AT^2$, which is a typical behavior of Fermi liquid systems. The values of A are plotted in the inset of figure 10 as a function of applied field. There is a shoulder in the $A - H$ curve at $H = 0.3$ T, corresponding to the metamagnetic transition, which was not observed in the $A - H$ curve for $H\|c$, as shown in figure 8. At $H = 3$ T, the A value decreases by 75% of the value at $H = 0$. The rapid decrease of A indicates that the electron-electron correlation is strongly suppressed by the application of magnetic field along the b-direction.

3.3. Specific heat

In figure 11, low temperature specific heat C of YbPdSi under applied magnetic fields of $H\|c$ and $H\|b$ are summarized. Figure 11(A) shows C/T of YbPdSi for $H\|c$ as functions of T. A sharp peak corresponding to the magnetic transition is observed for $H = 0$ T at $T_m = 8$ K. When a magnetic field is applied along the c-direction, the peak in C/T is rapidly suppressed and turns to a broad maximum. This broad peak shifts to higher temperatures with the increase of H, as is seen in figure 11(A). Similar behavior was previously observed for the measurement using a polycrystalline sample, and was explained by the Schottky behavior, where the magnetic field causes the Zeeman splitting of the lowest crystal field level of $J = 7/2$ in Yb^{3+} into two singlets, and the energy gap becomes wider with the increase of applied field. In this region, magnetic transition temperature is no more defined, like in many ferromagnetic materials under fields.

Below 3 K, C/T shows a downward decrease. This behavior is more clearly seen in figure 11(B), where C/T are plotted against T^2. The slope of C/T against T^2 changes at around 3 K, below which C/T decreases more rapidly than that does above 3 K. At present, it is not clear if this change in the slope is related to the broad maximum in the magnetic susceptibility along the b-direction at 3 K, that was shown in figure 4(A).

Many heavy fermion systems exhibit Fermi-liquid behavior, where the low temperature specific heat is described as:

$$C/T = \gamma + \beta T^2. \quad (1)$$

Here, γ is the electronic specific heat coefficient, and β is a constant related to the Debye temperature. For YbPdSi under $H\|c$, this behavior is not clearly observed. The fitting with equation (1) was applied only for the data below 3 K, as are shown in figure 11(B) with dotted lines.

Another possible explanation for the downward decrease in C/T below 3 K is that C obeys a power-low dependence $C \propto T^n$ with $n < 2$. In figure 11(C), the specific heat C are plotted against $T^{3/2}$. Here, C appear to be linear to $T^{3/2}$ in the temperature range from 1.8 to about 5 K. The $T^{3/2}$ dependence is consistent with the ferromagnetic spin wave contribution [22]. This effect can be dominant in low temperature specific heat of YbPdSi.

Specific heat of YbPdSi under $H\|b$ are also plotted in figure 11(D). The general trend is very similar to C for the case of $H\|c$: the sharp peak in C at $T_C = 8$ K becomes rapidly

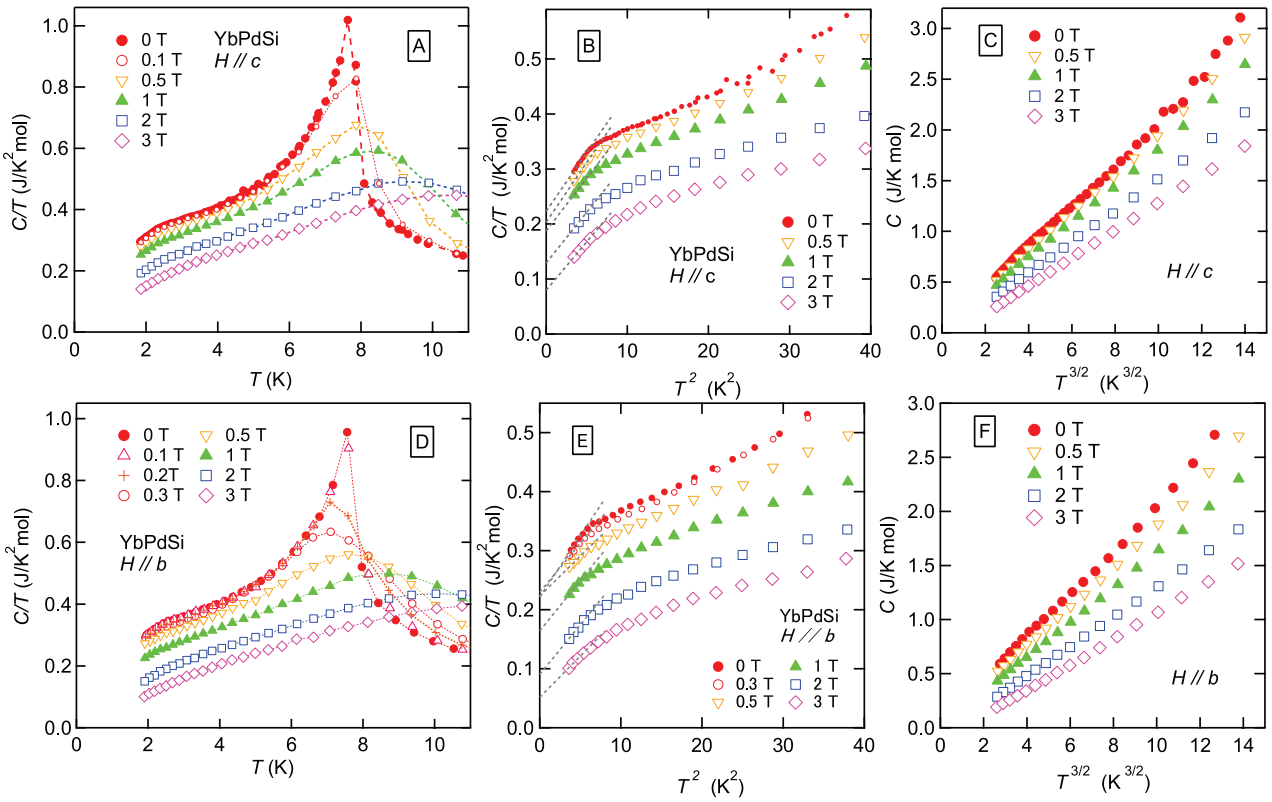

Figure 11. (A) Specific heat divided by temperature, C/T, of YbPdSi under magnetic field applied parallel to the c axis as a function of temperature T. (B) C/T of YbPdSi under $H\|c$ as a function of T^2. Dotted lines are results of the fit with $C/T = \gamma + \beta T^2$, where γ and β are constants. (C) C of YbPdSi under $H\|c$ as a function of $T^{3/2}$. (D) C/T of YbPdSi under $H\|b$ as a function of T. (E) C/T of YbPdSi under $H\|b$ as a function of T^2. Dotted lines are results of the fit with $C/T = \gamma + \beta T^2$. (F) C of YbPdSi under $H\|b$ as a function of $T^{3/2}$.

broadened by applying magnetic field. The peak in C shifts to a low temperature side up to $H = 0.3$ T. This shift of the transition temperature to lower temperatures under fields is consistent with the suppression of the antiferromagnetic components. Above 0.5 T, the peak in the C/T moves to higher temperatures, similarly to the case of $H\|c$, as shown in figure 11(A). This shift is explained by the increasing Zeeman splitting of the lowest doublet state by applied field.

C/T for $H\|b$ is plotted as functions of T^2 in figure 11(E). C/T shows a downward behavior against T^2, similarly to the case of $H\|c$, and follows equation (1) in a very narrow temperature range, below about 3 K. This can correspond to the broad maximum in the magnetic susceptibility shown in figure 4(A), similarly to the case of $H\|c$. On the other hand, C appears to follow the $T^{3/2}$ behavior as shown in figure 11(F), indicating the dominant ferromagnetic spin-wave contribution.

Values of γ obtained by the fitting of the C/T data using equation (1) are plotted in figure 12. Since the temperature range of the fitting was narrow, the values of γ contain large errors. γ shows a monotonic decrease with field for the case of $H\|c$. On the other hand, γ for $H\|b$ exhibits a slight maximum at $H = 0.3$ T, above which it decreases rapidly. These behavior is in very good accordance with the field dependence of the coefficient A of the electrical resistivity, as was shown in the insets of figures 8 and 10; A decreases monotonically for $H\|c$, whereas A exhibits a shoulder at 0.3 T for $H\|b$. These behavior reflects a close coupling between the electronic mass and the antiferromagnetic component in YbPdSi.

The Kadowaki–Woods ratio, A/γ^2, is calculated to be $A/\gamma^2 = 2.5 \times 10^{-5} \mu\Omega$ cm (K mol mJ)$^{-2}$ at $H\|c = 0$ T. This value is very close to those of many heavy fermion compounds with the doublet ground state degeneracy [23, 24].

3.4. Neutron powder diffraction

Figure 13 shows the neutron powder diffraction patterns of YbPdSi at 1.5 and 15 K. Both patterns agree very well, as can be seen in figure 13(A). The difference pattern between the two temperatures, $I_{\rm diff} = I_{1.5\,\rm K} - I_{15\,\rm K}$, is plotted in figure 13(B). $I_{\rm diff}$ is considered to be originated from the magnetic reflections, as will be explained below. All the peaks of the difference pattern agree with the position of the nuclear reflections, as can be seen in figure 13(B), which shows that the propagation vector of the magnetic structure is $k = (0, 0, 0)$. The largest intensity of $I_{\rm diff}$ is about 5×10^3 counts for the (0 1 1) reflection at $2\theta = 22$ degree, which is only 1% of the largest reflection of the nuclear reflection. This is sometimes the case for Yb compounds because of the large nuclear scattering length of Yb.

From figure 13(B), it is seen that the peak intensity of the (0 1 1) reflection is almost zero at $T = 15$ K. Hence, the temperature variation of the (0 1 1) reflection was investigated and is plotted in figure 14. It is seen that the peak intensity $I_{0\,1\,1}$ decreases with the increase of temperature, and becomes zero at $T_{\rm C} = 8$ K. Furthermore, the temperature dependence of $\sqrt{I_{0\,1\,1}}$, shown in figure 14(B), is well parallel to the

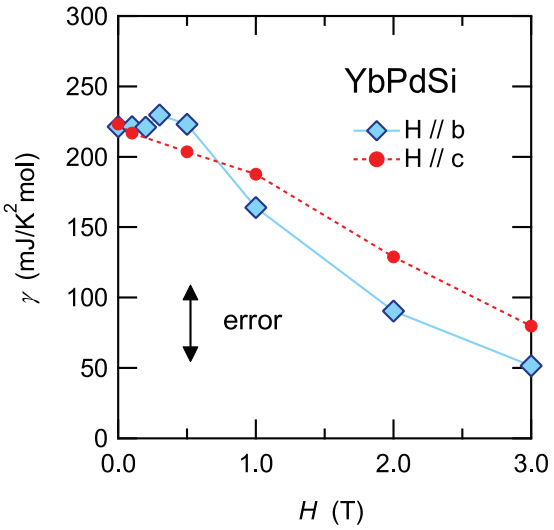

Figure 12. Electronic specific heat coefficient γ of YbPdSi as a function of magnetic field. The values of γ were derived by a fitting shown in figures 11(B) and (E) using the equation $C/T = \gamma + \beta T^2$.

temperature dependence of M_C, shown in figure 2(B). From these facts, we conclude that the difference pattern I_{diff} originates from the magnetic ordered moment of YbPdSi.

In order to investigate the magnetic structure that accords with the space group *Pmmn* and the propagation vector $k = (0, 0, 0)$, we employed the group theory analysis. In table 1, the irreducible representations (IR) for allowed magnetic structures are summarized. In the table, direction of the magnetic moment at Yb sites are shown by the vectors (u, v, w). There are eight candidates for the irreducible representations, from Γ_1 to Γ_8. Among them, only the Γ_7 representation gives rise to ferromagnetic moments along the c-direction. In addition, an antiferromagnetic component along the b-direction is also allowed in Γ_7, as is shown in the table. This is in good agreement with the antiferromagnetic-like behavior for $H \| b$ in YbPdSi observed by the magnetization measurements. Therefore, we performed Rietveld fitting based on the Γ_7 irreducible representation.

The analysis of the magnetic structure was carried out on the difference pattern I_{diff}, since the magnetic reflections are very weak. Firstly, neutron powder diffraction data at 15 K was analyzed by the Rietveld method (see figure S2 in the supplementary data), and the parameters such as the scale factor, lattice constants, atomic coordinates, and the peak profile parameters were refined. Then, fixing the parameters to the values at 15 K, only the magnitudes of magnetic components were refined on the difference pattern. In figure 15, the results of the Rietveld fitting of the difference pattern based on the Γ_7 irreducible representation is plotted by a thick green line. The calculated pattern explains the magnetic reflections very well, considering that only the magnetic moments were the fitting parameters. The magnetic moments along the c-direction were obtained from the fitting to be $m \| c = 0.26(3)\ \mu_B$, $1.30(4)\ \mu_B$, and $0.15(4)\ \mu_B$ for Yb1, Yb2, and Yb3 sites, respectively. The mean ferromagnetic moment is calculated to be $M_{ave} = (4m\|c(\mathrm{Yb1}) + 2m\|c(\mathrm{Yb2}) + 2m\|c(\mathrm{Yb3}))/8 = 0.49\ \mu_B$ per Yb. This

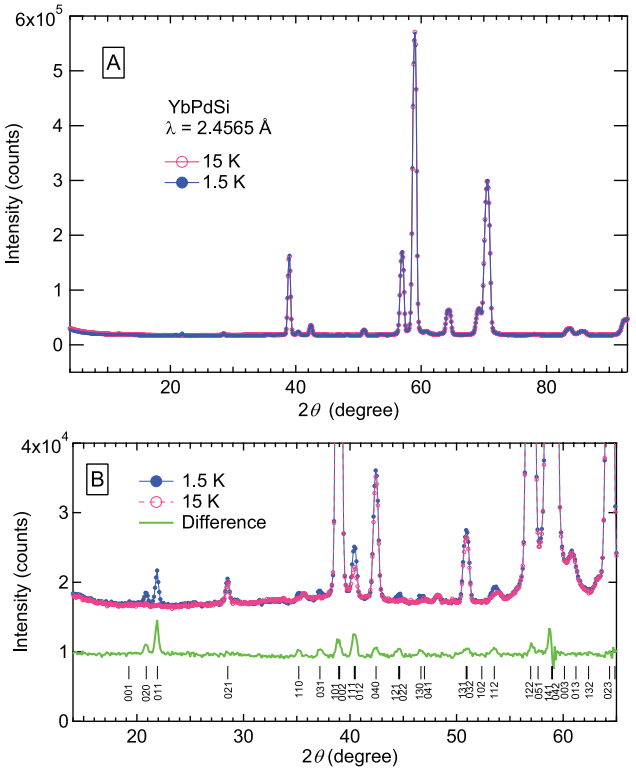

Figure 13. Neutron powder diffraction patterns of YbPdSi taken at 15 and 1.5 K. The difference of these patterns, $I_{diff} = I_{1.5\,K} - I_{15\,K}$, is plotted in the lower panel (B).

value is in a very good agreement with the observed magnetization, shown in figure 3(C). The antiferromagnetic component exists on the Yb1 site, with the value $m_b = 0.64(3)\ \mu_B$ per Yb. This fitting yielded $R_p = 26.0\%$, $R_{wp} = 35.3\%$, and the magnetic R-factor was 26.2%.

In figure 15, a fitting result based on a collinear ferromagnetism without antiferromagnetic components is also plotted by a blue broken line. Although the collinear model also gave a qualitative agreement with the observed data, the agreement is poor for (0 1 1), (1 1 1), (1 3 1), (0 3 2), (1 1 2), and (0 5 0) reflections. The R factors for this fitting were $R_p = 34.5\%$, $R_{wp} = 45.8\%$, and the magnetic R-factor 49.9%, much larger than those for the Γ_7 model shown above. Hence, we can conclude that the Γ_7 model with an antiferromagnetic component along the b-direction is more appropriate for the actual magnetic structure of YbPdSi than the collinear ferromagnetic model.

In the Γ_7 model, antiferromagnetic component occurs at the Yb1 ($4e$) site, and the Yb2 and Yb3 sites only have ferromagnetic moments along the c-direction. We examined the possibility where Yb2 ($2b$) and Yb3 ($2a$) may also have antiferromagnetic component in addition to the ferromagnetic moment. This can be modeled by taking a linear combination of Γ_7 with other irreducible representation. In table 1, Γ_4 can yield antiferromagnetic component along the b-direction at Yb2 and Yb3 sites. Then we performed a fitting using the linear combination of Γ_7 and Γ_4 for Yb2 and Yb3 sites, and only Γ_7 for Yb1 site. However, this fitting did not show any convergence. Therefore, we were unable to discuss the probability of this model.

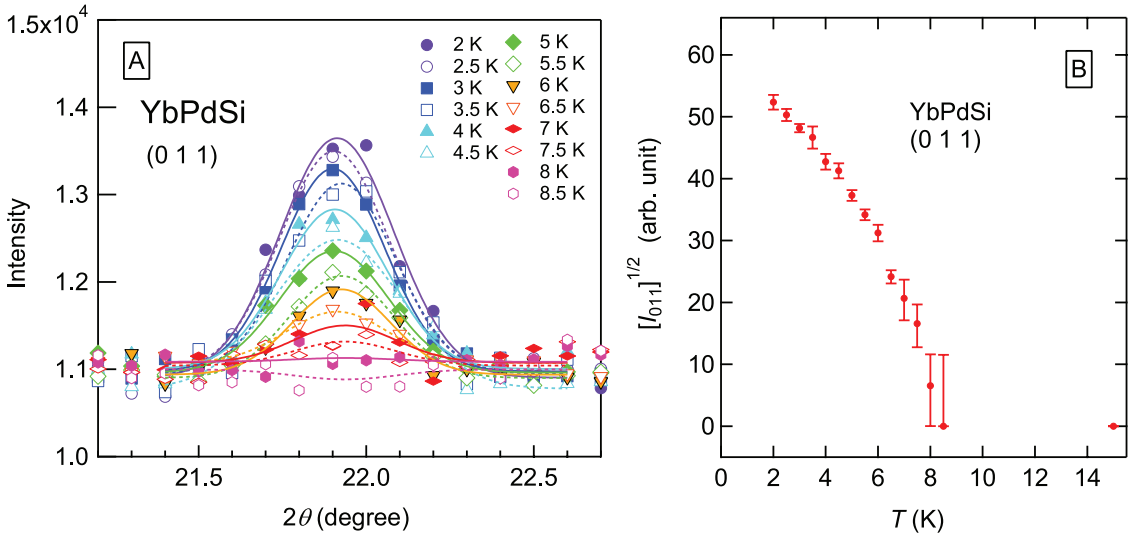

Figure 14. (A) Temperature variation of the (0 1 1) reflection in the neutron powder diffraction patterns of YbPdSi. Lines represent the fit with a Gaussian function. (B) Square root of the (0 1 1) peak intensity, $\sqrt{I_{011}}$, as a function of temperature.

Table 1. Magnetic arrangements of YbPdSi allowed for each of the irreducible representations (IR), calculated using the group theory analysis.

	Yb1 (4e)				Yb2(2b), Yb3(2a)		
IR	1/4, *y*, *z*	1/4, $-y+1/2$, *z*	3/4, $y+1/2$, $-z+1$	3/4, $-y+1$, $-z+1$	*x*, *y*, *z*	$-x+1$, $y+1/2$, $-z+1$	Magnetic type
Γ_1	*u*, 0, 0	$-u$, 0, 0	$-u$, 0, 0	*u*, 0, 0	No magnetic moment		AF‖*a*
Γ_2	0, *v*, *w*	0, $-v$, *w*	0, *v*, $-w$	0, $-v$, $-w$	0, 0, *w*	0, 0, $-w$	AF‖*ab*
Γ_3	*u*, 0, 0	*u*, 0, 0	*u*, 0, 0	*u*, 0, 0	*u*, 0, 0	*u*, 0, 0	F‖*a*
Γ_4	0, *v*, *w*	0, *v*, $-w$	0, $-v$, *w*	0, $-v$, $-w$	0, *v*, 0	0, $-v$, 0	AF‖*bc*
Γ_5	0, *v*, *w*	0, *v*, $-w$	0, *v*, $-w$	0, *v*, *w*	0, *v*, 0	0, *v*, 0	F‖*b* + AF‖*c*
Γ_6	*u*, 0, 0	*u*, 0, 0	$-u$, 0, 0	$-u$, 0, 0	*u*, 0, 0	$-u$, 0, 0	AF‖*a*
Γ_7	0, *v*, *w*	0, $-v$, *w*	0, $-v$, *w*	0, *v*, *w*	0, 0, *w*	0, 0, *w*	F‖*c* + AF‖*b*
Γ_8	*u*, 0, 0	$-u$, 0, 0	*u*, 0, 0	$-u$, 0, 0	No magnetic moment		AF‖*a*

Note: Yb1 atoms occupy the 4*e* site, which has 4 positions in the unit cell, (1/4, *y*, *z*), (1/4, $-y+1$, *z*), (3/4, $y+1/2$, $-z+1$), and (3/4, $-y+1$, $-z+1$). Yb2 atoms are on the 2*b* site, which has the atomic coordinates (1/4, 3/4, *z*) and (3/4, 1/4, $-z+1$). Yb3 atoms are situated on the 2*a* site, (1/4, 1/4, *z*) and (3/4, 3/4, $-z+1$). Values of *y* and *z* were refined by the Rietveld method using the neutron diffraction data at 15 K (see table S1 in the supplementary data (stacks.iop.org/JPhysCM/28/336002/mmedia)). Values of *u*, *v*, *w* in the table indicate the magnetic components parallel to the *a*-, *b*-, and *c*-directions, respectively. F and AF indicate ferromagnetic and antiferromagnetic components, respectively.

Another possibility for the antiferromagnetic component at the Yb2 and Yb3 sites is that each of the sites has Γ_5-type ferromagnetic component along the *b*-axis but pointing to the opposite direction each other. Thus we fit the diffraction pattern based on the Γ_7 type representation for Yb1 and the linear combination of Γ_7 and Γ_5 for Yb2 and Yb3, with the opposite sign of magnetic moment along the *b*-axis for Yb2 and Yb3 sites. This fitting yielded ferromagnetic components along the *c*-axis for Yb1, Yb2, and Yb3 to be $m_c = 0.30(3)$, 1.27(7), and 0.24(7) μ_B, respectively. The antiferromagnetic component for Yb1 is $m_b = 0.62(3)$ μ_B, while that for Yb2 and Yb3 sites are $m_b = \pm 0.29(10)$ μ_B. Although these values appear to be reasonable, the errors for the antiferromagnetic component of Yb2 and Yb3 sites are much larger than the case of the pure Γ_7-type structure. Furthermore, this fitting gave $R_p = 27.5\%$, $R_{wp} = 37.3\%$, and the magnetic *R*-factor 27.2%. These values are also larger than those obtained from the Γ_7 fitting. Therefore, existence of antiferromagnetic components at the Yb2 and Yb3 sites is not supported from our experimental results.

Figure 16 shows the magnetic structure of YbPdSi determined by the neutron powder diffraction and the Rietveld fittings. The magnetic moment at the Yb3 site is very small (0.15 μ_B), suggesting that the shielding by the conduction electrons via the Kondo effect affects strongly at this site. The heavy fermion behavior of YbPdSi can mainly be attributed to the strong Kondo screening at the Yb3 site. In addition, antiferromagnetic spin fluctuation at the Yb1 site can also be important for the heavy fermion behavior.

It is notable that the metamagnetic behavior (figure 5(B)) and the peak in the magnetoresistance (figure 9, inset) were observed only below 3 K. This may imply that the antiferromagnetic correlation develops below 3 K, and a collinear

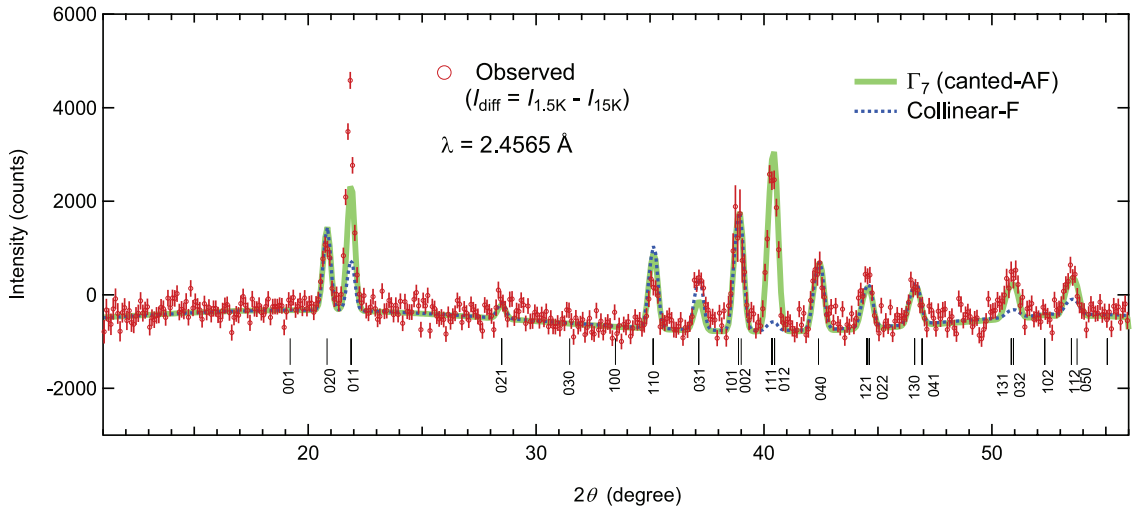

Figure 15. Results of the Rietveld fitting for the magnetic structure of YbPdSi. Circles indicate the observed data, I_{diff}, which is the difference intensity between 1.5 and 15 K. Thick green line is the fit based on the Γ_7 irreducible representation, which includes ferromagnetic moments along the *c*-axis and an antiferromagnetic component at the Yb1 site along the *b*-axis. Blue broken line represents the fit based on a collinear ferromagnetic model along the *c*-axis without antiferromagnetic components.

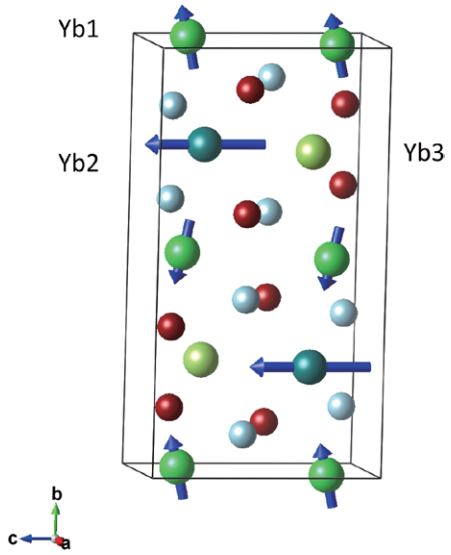

Figure 16. Magnetic structure of YbPdSi determined by the neutron powder diffraction. The arrows are drawn so their lengths are proportional to the magnetic moments. The arrow length at the Yb3 site is smaller than the diameter of the Yb atom.

ferromagnetism may be stable above this temperature. To clarify this possibility, we performed a Rietveld fitting using the difference pattern, $I_{4\,K} - I_{8\,K}$. However, the analysis suggested that the canted antiferromagnetic structure is more probable even at 4 K rather than a collinear-type one, as is shown in figure S3 in the supplementary data. The magnetic structure suggested by the fitting, hence, is essentially the same as that of figure 16, with an antiferromagnetic component at the Yb1 site along the *b*-direction. This is also supported by the temperature dependence of the (1 1 1) and (0 1 2) peak intensity, shown in figure S4 in the supplementary data. According to the Rietveld result shown in figure 15, the (1 1 1) and (0 1 2) peak intensity is mostly due to the antiferromagnetic component plus the nuclear reflections, and the contribution from the ferromagnetic component is very weak. We plotted the peak intensity of (1 1 1) and (0 1 2) as a function of temperature in figure S4. The result indicates that the peak intensity increases monotonically below $T_m = 8$ K, and no anomaly is seen around $T = 3$ K. This suggests that the antiferromagnetic component develops constantly below 8 K. At present, it is unclear whether a modification of the magnetic structure occurs at around 3 K. Other experiments such as the ultrasonic absorption measurements, which is a very sensitive probe for the magnetic transition [25, 26], would be useful to reveal the possible phase boundary.

4. Conclusion

Physical properties of YbPdSi have been characterized in detail using single crystalline samples. We confirmed a magnetic transition at $T_m = 8$ K, below which ferromagnetic moments develop with a spontaneous magnetization $M_s = 0.5\ \mu_B$/Yb at 2 K. The ferromagnetic moments point to the *c*-direction, although the magnetic moments at paramagnetic state show an Ising-like anisotropy along the *b*-axis. Field dependence of the magnetization along the *b*-direction shows a weak metamagnetic behavior at $H_m = 0.3$ T below $T = 3$ K. Also, magnetoresistance (MR) measured below 3 K exhibits a maximum at $H_m = 0.3$ T for fields parallel to the *b*-direction, corresponding to the metamagnetic transition. On the other hand, MR for $H \| c$ shows a monotonic decrease with fields, consistent with the ferromagnetic moment along the *c*-axis. The observed magnetic behavior indicates that YbPdSi exhibits magnetic ordering with a ferromagnetic moment along the *c*-direction and an antiferromagnetic component along the *b*-direction.

Temperature dependence of the electrical resistivity is described by $\rho(T) = \rho_0 + AT^2$, which is a characteristic feature of heavy Fermion systems. The value of *A* decreases with fields much faster for $H \| b$ than for $H \| c$. This may suggest that the heavy fermion behavior is strongly related to the antiferromagnetic correlation, which collapses by the application of

H along the b-direction. Specific heat C can be described by the Fermi liquid behavior, $C/T = \gamma + \beta T^2$, for only a narrow temperature range. Instead, $C \propto T^{3/2}$ was applicable for a wider temperature range. Although this is consistent with the dominant ferromagnetic spin wave contribution, another possibility of a phase transition around 3 K is not neglected.

Neutron powder diffraction revealed that the magnetic reflections appear only at the position of the nuclear reflections, suggesting the propagation wave vector $k = (0, 0, 0)$. Candidates for the magnetic structure were derived using the group theory analysis. Among possible irreducible representations, only the Γ_7-type model agrees with the ferromagnetic moment along the c-direction. Rietveld fitting based on the Γ_7 model yielded the magnetic structure with a mean ferromagnetic moment of $m_c = 0.49\ \mu_B$ along the c-axis, in a good agreement with the magnetization measurements. The analysis also yielded the antiferromagnetic component on the Yb1 site along the b-axis of $m_b = 0.64\ \mu_B$ per Yb. The magnetic moment at the Yb1 and Yb3 sites were small, $m_c = 0.26$ and $0.15\ \mu_B$, respectively, pointing to the c-direction. These reduced moments indicate the strong Kondo screening effect taking place for these two sites. Hence, the heavy fermion behavior can be attributed to the Kondo effect at the Yb1 and Yb3 sites. In addition, the rapid decrease of the A value in the electrical resistivity for $H \| b$ implies that the collapse of the antiferromagnetic component leads more detrimental effect on enhanced mass, similarly to YbPtGe and YbNiSn. Thus, the antiferromagnetic correlation plays a very important role for the formation of heavy fermion state in many ferromagnetic Kondo-lattice compounds.

Acknowledgments

The neutron powder diffraction experiments were performed at the cold neutron powder diffractometer (DMC) in the Swiss Spallation Neutron Source (SINQ), Paul Scherrer Institut (PSI). Illustrations of the magnetic structure (figure 16) was drawn with the VESTA software [27]. This work was partly supported by Grants-in-Aid for Scientific Research from Japan Society for the Promotion of Science, No. 15K05190.

References

[1] Stewart G R 2001 *Rev. Mod. Phys.* **73** 797
[2] Löhneysen H V 1999 *J. Magn. Magn. Mater.* **200** 532
[3] Gegenwart P, Si Q and Steglich F 2008 *Nat. Phys.* **4** 186
[4] Si Q and Steglich F 2010 *Science* **329** 1161
[5] Saxena S S *et al* 2000 *Nature* **406** 587
[6] Aoki D, Huxley A, Ressouche E, Braithwaite D, Flouquet J, Brison J P, Lhotel E and Paulsen C 2001 *Nature* **413** 613
[7] Aoki D and Flouquet J 2012 *J. Phys. Soc. Japan* **81** 011003
[8] Huy N T, Gasparini A, de Nijs D E, Huang Y, Klaasse J C P, Gortenmulder T, de Visser A, Hamann A, Görlach T and Löhneysen H V 2007 *Phys. Rev. Lett.* **99** 067006
[9] Gupta S and Suresh K G 2015 *J. Alloys Compd.* **618** 562
[10] Tsujii N and Kitazawa H 2013 *Solid State Commun.* **159** 65
[11] Prots' Y M, Pöttgen R and Jeitschko W 1998 *Z. Anorg. Allg. Chem.* **624** 425
[12] Kasaya M, Tani T, Kawate K, Mizushima T, Isikawa Y and Sato K 1991 *J. Phys. Soc. Japan* **60** 3145
[13] Itoh Y and Kadomatsu H 1998 *J. Alloys Compd.* **280** 39
[14] Katoh K, Nakagawa S, Terui G and Ochiai A 2009 *J. Phys. Soc. Japan* **78** 104721
[15] Katoh K, Heying B, Hoffmann R D, Rodewald U C and Pöttgen R 2008 *Z. Anorg. Allg. Chem.* **634** 1296
[16] Enoki K *et al* 2012 *J. Phys. Soc. Japan* **81** SB056
[17] Katoh K, Koga T, Terui G and Ochiai A 2010 *J. Phys. Soc. Japan* **79** 084709
[18] Tsujii N, Katoh K, Keller L, Dönni A, Terada N and Kitazawa H 2015 *J. Phys.: Condens. Matter* **27** 325601
[19] Rodrigues-Carvajal J 1993 *Physica* B **192** 55
[20] Wills A S 2000 *Physica* B **276** 680
[21] Yamada K 2004 *Electron Correlation in Metals* (Cambridge: Cambridge University Press)
[22] Ziman J M 1972 *Principles of the Theory of Solids* (New York: Cambridge University Press)
[23] Kadowaki K and Wods S B 1986 *Solid State Commun.* **58** 507
[24] Tsujii N, Kontani H and Yoshimura K 2005 *Phys. Rev. Lett.* **94** 057201
[25] Ishii I, Noguchi Y, Kamikawa S, Goto H, Fujita T K, Katoh K and Suzuki T 2014 *J. Phys. Soc. Japan* **83** 043601
[26] Xi X, Ishii I, Noguchi Y, Goto H, Kamikawa S, Araki K, Katoh K and Suzuki T 2015 *J. Phys. Soc. Japan* **84** 124602
[27] Momma K and Izumi F 2011 *J. Appl. Crystallogr.* **44** 1272